Research Article

Elhassan El Bahraoui*, Lahcen Khouchaf, Abdelhamid Oufakir, Amor Ben Fraj, Mohammed Elaatmani, and Abdelouahed Zegzouti

Nano-structural and nano-constraint behavior of mortar containing silica aggregates

https://doi.org/10.1515/rams-2022-0027 received October 10, 2021; accepted February 17, 2022

Abstract: In this study, nano-structural and nano-constraints behavior of two silica aggregate mortars are investigated. The first silica aggregate (A) is almost pure silica and the second one (B) contains silica, calcite and dolomite phases. The relationship between the durability and nano-structural changes is evidenced using Transmission Electron Microscope, X-ray diffraction (XRD) and TGA/DTA. The nano-structural results show that the macroscopic properties of mortars greatly depend on physico-chemical properties of aggregates. Higher the water absorption, higher the consumption of the Portlandite; the consumption of Portlandite, after 28 days of curing, is more in Bm sample than in Am sample. A relationship between the Portlandite content and the water absorption is evidenced. The relationship between reactivity and nano-constraints deduced from XRD modeling is highlighted.

Keywords: durability, natural silica aggregates, Portlandite, nano constraints, TEM

1 Introduction

Recently, a range of modification methods have been proposed to improve the properties of recycled aggregate

* Corresponding author: Elhassan El Bahraoui, Department of Chemistry, Laboratory of Materials Science and Process Optimization, Cadi Ayyad University, Semlalia Faculty of Science, Marrakech, Morocco, e-mail: h.elbahraoui@gmail.com

Lahcen Khouchaf: Research Center, IMT Nord Europe, Lille University, Cité Scientifique, Rue Guglielmo Marconi, BP 20145, 59653 Villeneuve D'Ascq Cedex, France

Abdelhamid Oufakir, Mohammed Elaatmani,

Abdelouahed Zegzouti: Department of Chemistry, Laboratory of Materials Science and Process Optimization, Cadi Ayyad University, Semlalia Faculty of Science, Marrakech, Morocco

Amor Ben Fraj: Dima Team, Cerema Research Team DIMA, 120 Rue de Paris – BP 216, Sourdun, 77487 Provins Cedex, France

concrete (RAC). Zeng et al. showed that nano-silica (NS) improved the microstructure properties and enhanced the mechanical strength of RAC [1].

Seifan et al. investigated the influence of NS and micro-silica (MS) on the properties of fly ash-based geopolymer mortar. However the presence of 5% NS aids in the strength development over 28 days [2].

Other recent studies have shown interest in SiO2 compounds and the impact of steel fibers and silica fume (SF) on the mechanical properties of RACs made of two different types of recycled coarse aggregates sourced from both low-and high-strength concretes were evaluated [3,4]. In addition, silica compounds have several applications in different areas [5,6]. Natural SiO₂ aggregates and Pozzolanic materials are frequently used in the construction industry because of their low production cost and their significant reduction in CO₂ emissions. Their use improves the durability because of the low permeability [7,8]. These materials improve both strength and durability of mortars and concrete by their reaction with calcium hydroxide and production of calcium silicate hydrate in the pore structure [9–11]. It can affect the durability of concrete structures, and lead to expansion, cracking and deterioration of concrete [12,13]. Recycled coarse aggregate are also used in cement and in concrete [14,15]. The durability of concrete has been a matter of interest for researchers in the past decades, and throughout their numerous research works [16-18]. Some studies have shown that the addition of SiO2 nanoparticles allows an improvement in the mechanical properties of the material [19]. On the other hand, the addition of the nanoparticles will have negative consequences on the environment during the wear of the material and the release of those nanoparticles in nature. The addition of natural silica to cement matrix can improve the electrical resistivity of concrete not only by refinement of pore structure, but also by consuming of Portlandite Ca(OH)₂ and causing a reduction in OH content in pore solution, which decreases the conductivity of the specimens [19].

To improve the durability of the material, a study is underway based on heat treatments [20] without addition

of new compounds. However, in order to optimize the choice of the aggregates to use, it is important to understand the relationship between chemical composition, the microstructure of incorporated aggregates and the reactivity.

Two main properties, crystallite size and lattice strain, would affect Bragg peak width, intensity of peak and shift of the 2θ peak position accordingly [12]. Therefore, the crystallite size and lattice strain can be deduced by analyzing the peak width. Crystallite size is a measure of the size coherent to diffracting domain. The crystallite size of the particle is not generally the same as the particle size due to the presence of polycrystalline aggregates [6]. Lattice strain is a measure of the distribution of lattice constants arising from crystal imperfections, such as lattice dislocation. The other sources of strain are grain boundary triple junction, contract or sintered stresses, stacking faults and coherency stresses [9].

It should be noted that apart from the evident fact that elastic properties are key mechanical properties of their own, they determine the maximum strength and hardness of the materials and significantly affect the thermal shock behavior of the materials. There are many analytical techniques to evaluate the microstructure properties of the materials [13,21]. To our knowledge, they do not resolve many physical issues leading to the change in the structural properties of SiO₂ materials. In this regard, this article investigates the effect of heat treatment on microstructure morphology of SiO₂ flint by Williamson–Hall plots methods namely Williamson–Hall-isotropic strain model (W–H-ISM).

In this study, two silica aggregates with different origins are studied. It is also essential to monitor the effect of the chemical composition of the aggregate on its reactivity. The chemical compositions are different, one is practically a pure SiO_2 and the second has a predominantly SiO_2 phase with the presence of calcite and dolomite. The novelty of this research work is to investigate the relationship between the water absorption of aggregates and the Portlandite content of the mortar. In addition, the relationship between reactivity and micro constraints is explored.

2 Experimental program

2.1 Theoretical background of W-H-ISM

In order to understand the contributions of lattice strain and crystalline size to the X-ray diffraction (XRD) peaks, the Williamson–Hall method is used. The lattice strain and crystallite size were estimated by W–H-ISM, based on Williamson–Hall (W–H) plot from powder XRD data.

Equation (1) gives an estimate of lattice isotropic strain and crystallite size (D_{W-H}) by W-H-ISM:

$$\beta \cdot \cos \theta = \frac{0.9\lambda}{D_{W-H}} + 4\varepsilon \cdot \sin \theta.$$
 (1)

Here equation (1) stands where it is assumed that strain is uniform in all crystallographic directions. The strain (ε) present in the materials and the crystallite size $(D_{\rm W-H})$ are, respectively, determined from the slope and *y*-intercept of the fitted line.

The conventional W–H-ISM model is an appropriate approach for the estimate of lattice strain due to less scatter of data points from the linear fit. The better fit of the experimental data points confirms the uniformity of the lattice strain.

In many cases, the materials cannot have identical values of a property in all directions. Stress and strain relations with elastic behavior are described by Hooke's law, which is valid only up to the proportionality limit of a material. Beyond this limit, Hooke's law no longer applies. There exists linear proportionality relation between stress and strain and is given by $\sigma = \varepsilon E$, where E is the constant of proportionality being the modulus of elasticity or Young's modulus. Williamson–Hall equation (2) could be written in another way:

$$\beta \cdot \cos \theta = \frac{0.9\lambda}{D_{\text{W-H-ASM}}} + \frac{4\sigma \cdot \sin \theta}{E_{hkl}},$$
 (2)

where σ is the uniform stress and E_{hkl} is the Young's modulus in the direction perpendicular to the set of crystal lattice planes (h k l). The crystallographic direction dependent on Young's modulus in hexagonal crystals [22] is given by equation (3):

$$E_{hkl} = \frac{\left[h^2 + \frac{(h+2k)^2}{3} + \left(\frac{al}{c}\right)^2\right]^2}{s_{11}\left(h^2 + \frac{(h+2k)^2}{3}\right)^2 + s_{33}\left(\frac{al}{c}\right)^4},$$

$$+ (2s_{13} + s_{44})\left(h^2 + \frac{(h+2k)^2}{3}\right)\left(\frac{al}{c}\right)^2}$$
(3)

where the Young's modulus E_{hkl} can be determined along any orientation, from the elastic constants (S_{ij}). Here S_{11} , S_{33} , S_{44} and S_{13} are the elastic compliances and their standard hand book values are 7.49×10^{-12} , 10.9×10^{-12} , 15.1×10^{-12} and -4.0×10^{-12} , respectively [23–25].

A scatter plot with a regression line of $\beta\cos\theta$ vs $4\sin\theta/E_{hkl}$ gives σ in the slope of the line, and $D_{W-H-ASM}$ is calculated from the $\beta\cos\theta$ -intercept.



Figure 1: Photographs and the preparation setup of the aggregates A and B.

2.2 Materials

In this research, two siliceous natural aggregates (called aggregate A and aggregate B) are used. The aggregate A is a rock type and the aggregate B is an alluvial type. In Figure 1, the photographs of the aggregates before and after grinding are presented. These aggregates are heterogeneous in appearance and the crystalline structure is based on quartz phase for aggregate A, and quartz as major component with calcite and dolomite phase for aggregate B. Both aggregates were first crushed using jaw crusher and sieved, before constituting the same granular skeleton of standardized sand (S). The physical properties of the tested sand are summarized in Table 1.

For standardized mortar (water-to-cement ratio [w/c] of 0.5) manufacturing, cement type CEM I 52.5 is used.

2.3 Methods

For their valorization in a cementitious material, standardized mortars are prepared according to NF (EN 196-1, 1995) [26]. In order to make effective water-to-cement ratio (w/c) constant, water for sands saturation is added in the mixer. The samples were analyzed by means of different techniques.

XRD measurements were performed in the reflection mode using a Bruker D8 Advance diffractometer (Cu-K λ radiation = 1.5418 Å), which operates at 40 kV and 40 mA. Data were collected in the range of 5–75° in the 2θ scale with a step size of 0.02° and a counting time of 0.5 s per step.

Nanostructure of samples were compared using a Transmission Electron Microscope (TEM). The investigation was performed with a FEI Tecnai G2-20 instrument with an accelerating voltage of 200 kV. This microscope is equipped with a filament of lanthanum hexaboride LaB6, a double holder, an energy dispersive X-ray spectroscopy analysis and Gatan digital camera CCD ORIUS.

To quantify the different phases, particularly calcite, quartz and Portlandite, thermogravimetric analysis/differential thermal analysis (TGA/DTA) tests are carried out on 250–300 mg samples. As for XRD, aggregates and mortars are powdered and sieved using 315 μ m sieve, before testing. Then, each sample is placed in Al₂O₃ crucible and a range of temperature 35–1,200°C is applied.

3 Results and discussion

3.1 Physical properties of studied sands

Figure 2 shows that the grains' size is between 0.1 mm and 2 mm as for a standardized sand.

In addition, parameters of the aggregates such as the density and water absorption are determined [27]. As shown in Table 1, sand B has a higher water absorption in comparison with sand A and the standardized one.

The water absorption property shows that the aggregate B is very porous compared to the aggregate A.

3.2 Nano-structural characterization of starting aggregates

3.2.1 TEM study

Figure 3 shows the TEM micrographs of sands A (Figure 3a) and B (Figure 3b). For both sands, the images show different

Table 1: Physical properties of the aggregates A, B and the sand S used as reference

	Туре	Water absorption (%)	Density (g⋅cm ⁻³)
Aggregate A	Natural aggregate	1.61	2.56
Aggregate B	Natural aggregate	2.28	2.75
Sand S	Standardized Sand	0.9	2.65

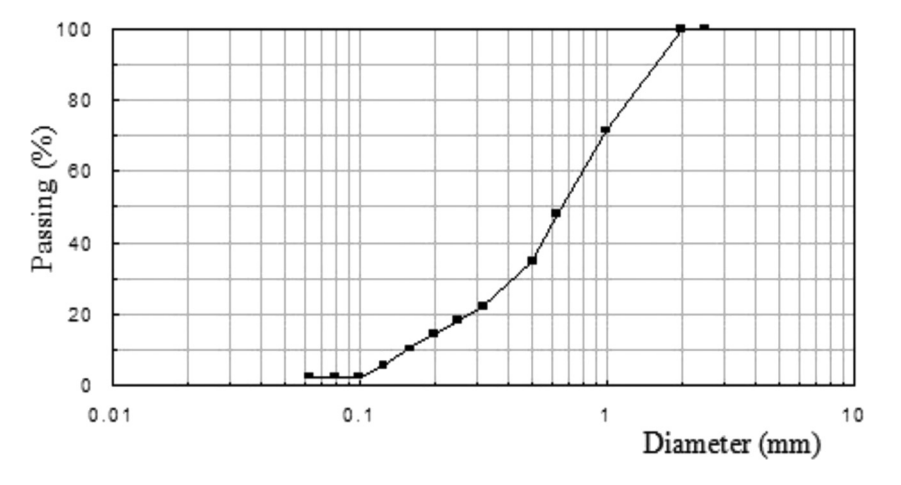


Figure 2: Size distribution of the aggregates used.

sizes of SiO_2 grains ranging from ten nanometers to a few micrometers, with angular sides characterizing angles of quartz phase. Moreover, for sample B, other areas of a rather disordered or amorphous appearance are observed. In addition, sand B seems to be more heterogeneous compared to aggregate A.

The distribution and the shape of the particles are different in the two samples. Thus, it stands out that sample A exhibited more hexagonal shape particles. While the sample B consisted of spherical particles compared with the sample A particles. It is clear that the external nano and microstructure part of sample B can indicate about its behavior in mortar as it will be stated below. While the nano and microstructure part of the sample A is quite similar among the core and the external surface.

3.2.2 XRD study of studied aggregates

XRD patterns of the aggregates A, B and the standardized sand are shown in Figure 4. The aggregates A and B have

different structures. The structure of the aggregate A is quite similar compared to the standardized sand (S). The aggregate A contains almost only the quartz phase, while aggregate B contains three phases: quartz (Q), calcite (C) and dolomite (D).

According to the XRD patterns, the quartz phase is the main component of the framework of aggregates A and B. The dolomite and calcite in aggregate B are present in minor phases but could influence its behavior.

3.3 Nano-structural characterization of manufactured mortars

Figure 5 shows the XRD patterns of the mortars based on aggregates A, B and Standardized Sand, respectively, named Am, Bm and Sm. Important differences were noticed in the sample Bm compared to the sample Am. The XRD patterns show that Bm presents the same phases as that of Am and Sm, but the peak of calcite phase is more pronounced. In addition, the Portlandite phase in

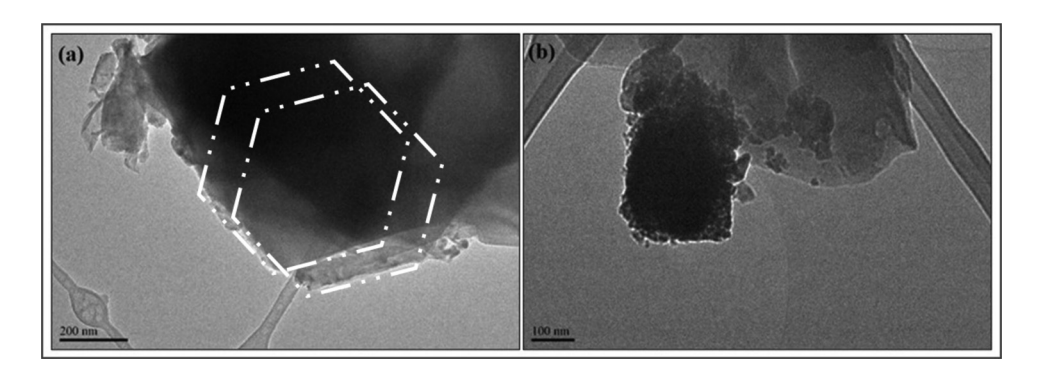


Figure 3: TEM micrographs of aggregates A (a) and B (b).

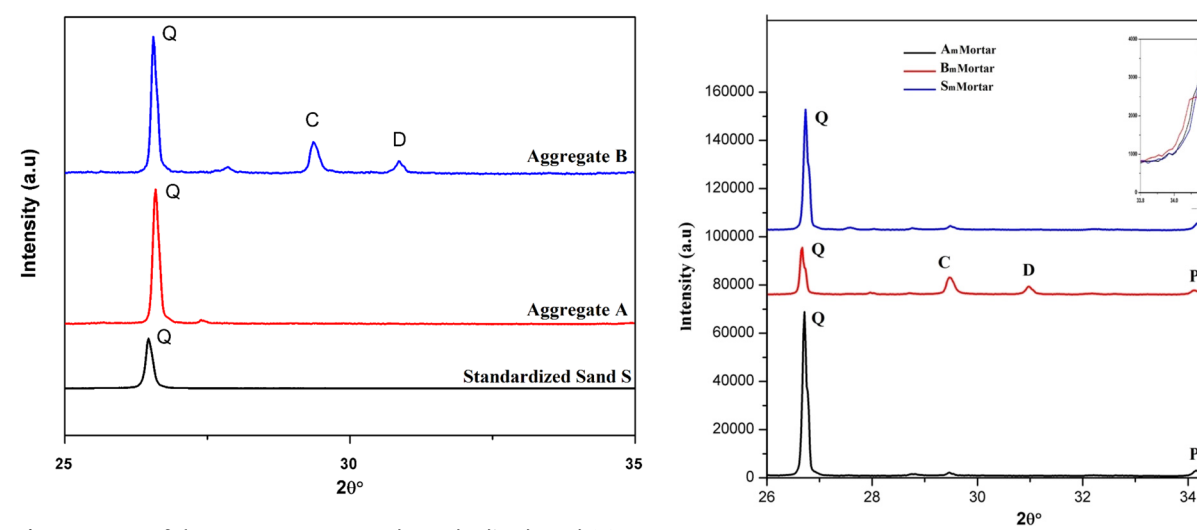


Figure 4: XRD of the aggregates A, B and standardized sand (S).

Figure 5: XRD of mortars Am, Bm and Sm samples.

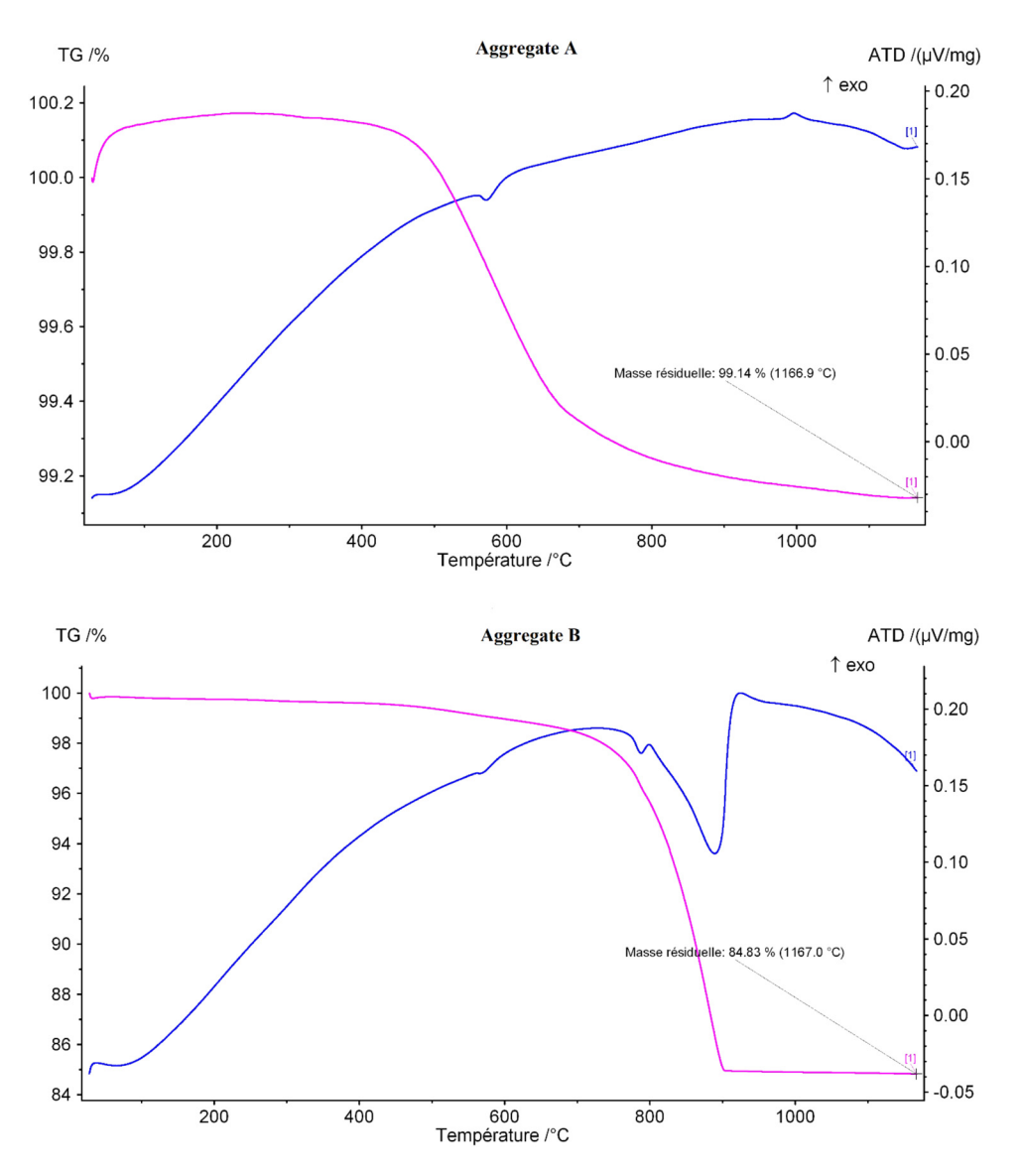


Figure 6: TGA/DTA of the aggregates A and B.

the Bm is lower compared to the Am and the Sm samples. This result can be partially explained by the water absorption values as indicated in Table 1, since the water absorption is greater in Bm than in Am and in Sm. The fact that less Portlandite was detected in the Bm sample is also representative of the more advanced interaction process in this sample.

Figure 6 shows the TGA/DTA diagrams corresponding to the aggregates A and B. It is noted that a mass loss in the temperature range [100–450°C] is due to dehydration of water contained in the aggregates. The weight loss is low for both the aggregates but is higher for aggregate B. This

fact is in agreement with the water absorption rate of the aggregates as seen in Table 1.

In addition, a sharp reduction in mass occurs in the temperature range [450–700°C]. The mass loss is 0.5% for aggregate A, unlike aggregate B which has no change in mass in this range of temperature. On the other hand, in the temperature range [700–900°C], there is a sudden change in the mass loss of aggregate B corresponding to a weight loss of 11% compared to a weight loss of 0.2% in aggregate A. This loss is linked to the decarbonation of calcite CaCO₃ present in aggregate B and is in agreement with the XRD results as shown above.

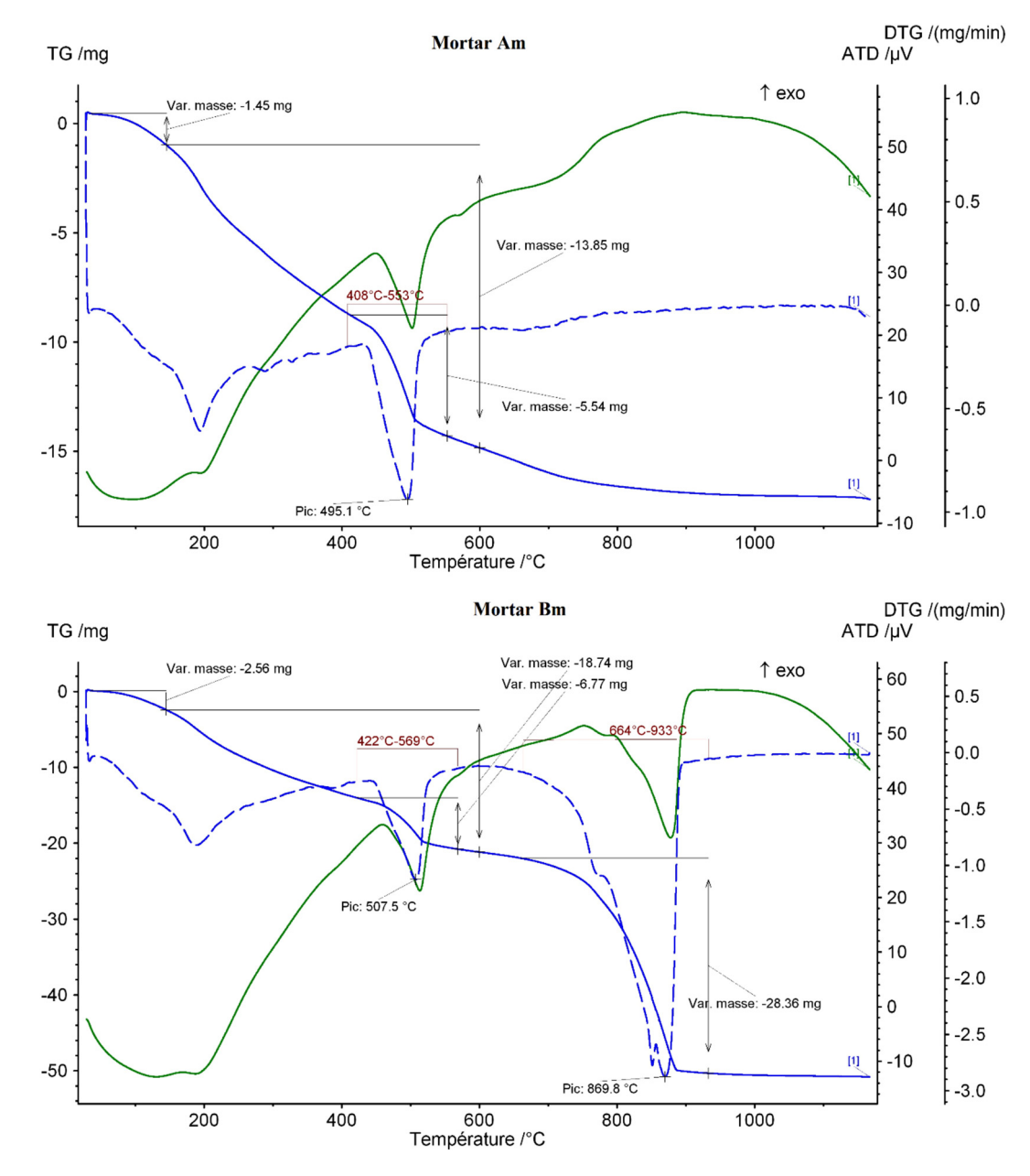


Figure 7: TGA/DTA of the mortars Am and Bm.

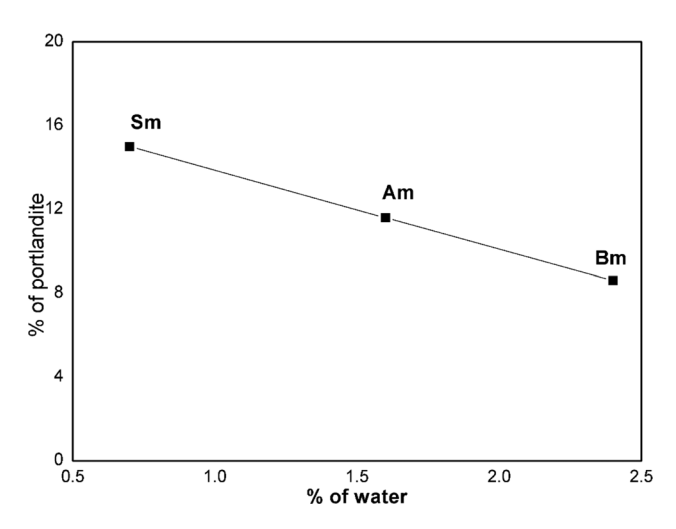


Figure 8: Relationship between the percentage of Portlandite in Am, Bm and Sm vs the water absorption.

In fact, at the temperature of 1,200°C, there is a loss of overall weight of 0.85% for aggregate A compared to 15% in aggregate B. This significant difference may explain the difference in terms of the reactivity and the durability between the two aggregates A and B (Figure 6).

Figure 7 shows TGA/DTA diagrams of Am and Bm. It is noted that there is a weight mass loss in the temperature range [100–450°C], that is related to the dehydration of water contained in the mortars. The mass loss is 4.5% in the Am compared to a mass loss of 5.5% in the Bm. It can be seen that there is more water with Bm than Am, which is in agreement with the results of water absorption of aggregates. The 2nd temperature interval is [400-520°C], that is related to the dehydration of the Portlandite Ca(OH)₂. A mass loss is about 2.5% for the Am compared to a mass loss of 1.5% for the Bm. Indeed, the Am contains more Portlandite than the Bm, which is in good agreement with the XRD results. The 3rd temperature interval is [700-900°C], which is relative to the decarbonation of the calcite CaCO₃ where the peak intensity is important on the DTA curve of the Bm mortar. The mass loss is about 0.2% in the Am compared to 10% in the Bm. This result is confirmed by XRD.

Table 3: Sizes of crystallites and micromechanical constraints for the starting aggregates and mortars

Methods	Parameters	Α	В	Am	Bm
W-H-ASM	D _{ASM} (nm)	90	90	95	97
	σ (MPa)	138.6	135.1	176.6	190.5

3.4 Relationship between Portlandite and water absorption

Figure 8 presents the decrease in Portlandite content (%) of different mortars with the increase in water absorption (%). As demonstrated previously by XRD (Figure 5) and TGA/DTA (Figure 7), the Portlandite content of Bm mortar is less than that of Am, while the water absorption in aggregate B is higher than that in aggregate A.

The results show that the presence of calcite in the starting aggregate B is associated with the water absorption increase in the samples. Calcite that cannot connect with concrete contribute to fill the spaces but they lead to a rise in permeability [8]. Thereby, the interaction between the solution and the aggregate increases which increase the consumption of the Portlandite in Bm compared to the Am.

3.5 Nano-constraints and crystal lattice parameters

Based on diffraction spectra, modeling was carried out to determine certain nano-structural and nano-mechanical properties of two natural aggregates and in mortars (Table 2) such as the volume of the unit cell, the size of the crystallites and the micro-stresses. It can be noted that the volume of the unit cell increases mainly for the Bm sample, which proves the swelling of its structure. This result could be linked to the value of higher water absorption in the aggregate that facilitates its reactivity by introducing species more easily through the pores. Likewise, Table 2 shows the value of the sizes of the

Table 2: FWHM, atomic parameters and the volume of the unit cell for the starting aggregates A and B, and Am and Bm mortars

Samples	Structure	FWHM of principal pic (101)	Parameters of lattice		Lattice volume (ų)
			$a = b (\mathring{A})$	c (Å)	
A	Hexagonal	0.1378	5.1166 ± 0.0001	5.4979 ± 0.0002	124.6493 ± 0.005
В		0.1181	5.1121 ± 0.0001	5.5031 ± 0.0002	124.5493 ± 0.005
Am		0.1378	5.1126 ± 0.0001	5.4965 ± 0.0002	125.4227 ± 0.005
Bm		0.1338	5.1142 ± 0.0001	5.5012 ± 0.0002	125.6066 ± 0.005

crystallites in both the aggregates (A and B) and in their respective mortars. The most important result is that this value is more important in the mortar. This result could be explained by the SiO_2 reaction in the mortar and only the well-crystallized areas resisted the reaction, which gives larger crystallite sizes. In the same way, the constraints are determined in the two starting aggregates and in mortar, Table 3. It can be seen that the stress values are greater in the mortar. Likewise, in mortar, the value of the constraint in the Bm mortar is greater compared to the Am mortar. This result can be linked to the greater value of the unit cell volume of this sample and to its reactivity that seems greater compared to that of aggregate A.

Indeed, the following table clearly shows the volume increase in the crystal unit cell of starting aggregate B compared to the starting aggregate A, which can be considered as a parameter of the reactivity of the starting aggregate B.

Table 3 shows that Bm mortar is more stressed than Am mortar in agreement with the fact that the aggregate B is more reactive than the aggregate A.

The magnitude of the constraint value (σ) is found around 176.6 MPa in Am mortar and 190.5 MPa in Bm mortar.

4 Conclusion

In this study, two natural silica aggregate mortars with different chemical composition are studied. We demonstrated that the Portlandite phase evolution is a good parameter to follow the aggregate behavior. A relationship between the Portlandite content and the water absorption is evidenced. In addition, conclusions from the experimental and analytical results are drawn as follows:

- Higher the water absorption, higher is the consumption of the Portlandite.
- The chemical composition of the two aggregates has a great effect on their reactivity.
- After 28 days, the Portlandite content is more important for Am than for Bm.
- Unlike the other phases, the dolomite phase completely disappeared from Bm mortar.
- There is a good agreement between macro and micromechanical strains and the reactivity.

Acknowledgments: Part of this research was funded European Community funding FEDER Institut Chevreul USTL-France, and Analysis and Characterization Center (CAC)-Morocco.

Funding information: Part of this research was funded by FEDER, Institut Chevreul USTL-France, and Analysis and characterization center (CAC)-Morocco.

Author contributions: Experimental procedure and the data processing: E.E., L.K., A.O., and A.B.; designing the experiment: L.K., H.E., A.B., M.E., and A.Z; participating in preparing the manuscript: L.K., E.E., and A.O.

Conflict of interest: The authors declare no conflict of interest

References

- Zeng, W., Y. Zhao, H. Zheng, and C. S. Poon. Improvement in corrosion resistance of recycled aggregate concrete by nano silica suspension modification on recycled aggregates. Cement and Concrete Composites, Vol. 106, 2020, id. 103476.
- [2] Seifan, M., S. Mendoza, and A. Berenjian. Mechanical properties and durability performance of fly ash based mortar containing nano- and micro-silica additives. *Construction and Building Materials*, Vol. 252, 2020, pp. 119–121.
- [3] Du, H. Properties of ultra-lightweight cement composites with nano-silica. *Construction and Building Materials*, Vol. 199, 2019, pp. 696–704.
- [4] Jahandari, S., M. Mohammadi, A. Rahmani, M. Abolhasani, H. Miraki, L. Mohammadifar, et al. Mechanical properties of recycled aggregate concretes containing silica fume and steel fibres. *Materials*, Vol. 14, 2021, id. 7065.
- [5] Chen, L. and D. F. Lin. Applications of sewage sludge ash and nano-SiO2 to manufacture tile as construction material. *Construction and Building Materials*, Vol. 23, 2009, pp. 3312–3320.
- [6] Khouchaf, L., A. Hamoudi, and P. Cordier. Evidence of depolymerisation of amorphous silica at medium and short range order: XANES, NMR and CP-SEM contributions. *Journal of H- Materials*, Vol. 168, 2009, id. 1188.
- [7] Kallel, T., A. Kallel, and B. Samet. Durability of mortars made with sand washing waste. *Construction and Building Materials*, Vol. 122, 2016, pp. 728-735.
- [8] Temiz, H. and F. Kantarcı. Investigation of durability of CEM II B-M mortars and concrete with limestone powder, calcite powder and fly ash. Construction and Building Materials, Vol. 68, 2014, pp. 517–524.
- [9] Khouchaf, L. and J. Verstraete. Multi-technique and multi-scale approach applied to study the structural behavior of heterogeneous materials: natural SiO₂ case. *Materials Science*, Vol. 42, 2007, pp. 2455–2462.
- [10] Pratap, S. L., A. Goel, S. K. Bhattachharyya, S. Ahalawat, U. Sharma, and G. Mishra. Effect of morphology and dispersibility of silica nanoparticles on the mechanical behaviour of cement mortar. *International Journal of Concrete Structures* and Materials, Vol. 9, No. 2, June 2015, pp. 207–217.
- [11] Khouchaf, L., K. Boulahya, P. P. Das, S. Nicolopoulos, V. K. Kis, and J. L. Lábár. Microstructure study of amorphous silica

- nanostructure using high resolution electron microscopy, electron energy loss spectroscopy, X-ray powder diffraction and electron pair distribution function. Materials, Vol. 13, 2020, id. 4393.
- [12] El Bahraoui, E., L. Khouchaf, and A. Benfraj. Microscopical and mechanical evaluation of the durability of SiO₂ aggregates. The European Physical Journal Applied Physics, Vol. 74, 2016, id. 24610.
- [13] Tahiri, N., L. Khouchaf, M. Elaatmani, G. Louarn, A. Zegzouti, and M. Daoud. Study of the thermal treatment of SiO2 aggregate. Materials Science and Engineering, Vol. 62, 2014, id. 012002, doi: 10.1088/1757-899X/62/1/012002.
- [14] Su, T., C. Wang, F. Cao, Z. Zou, C. Wang, J. Wang, et al. An overview of bond behavior of recycled coarse aggregate concrete with steel bar. Reviews on Advanced Materials Science, Vol. 60, 2021, pp. 127-144.
- [15] Meng, T., S. Lian, K. Ying, and H. Yu. Feasibility study of cement-stabilized materials using 100% mixed recycled aggregates from perspectives of mechanical properties and microstructure. Reviews on Advanced Materials Science, Vol. 60, 2021, pp. 490-502.
- [16] Najigivi, A., A. Khaloo, A. I. Zad, and S. A. Rashid. An artificial neural networks model for predicting permeability properties of nano silica-rice husk ash ternary blended concrete. International Journal of Concrete Structures and Materials, Vol. 7, No. 3, September 2013, pp. 225-238.
- [17] Hwan, S. J., V. Saraswathy, S. Karthick, P. Kathirvel, and S. J. Kwon. Microstructure characteristics of fly ash concrete with rice husk ash and limestone powder. International Journal of Concrete Structures and Materials, Vol. 12, No. 1, February 2018, id. 17.
- [18] Tittarelli, F., C. Giosuè, and A. Mobili. Recycled glass as aggregate for architectural mortars. International Journal of Concrete Structures and Materials, Vol. 12, 2018, id. 57.

- [19] Lavergne, F., R. Belhadi, J. Carriat, and A. Ben Fraj. Effect of nano-silica particles on the hydration, the rheology and the strength development of a blended cement paste. Cement and Concrete Composites, Vol. 95, 2019, pp. 42-55.
- Tufail1, M., K. Shahzada, B. Gencturk, and J. Wei. Effect of elevated temperature on mechanical properties of limestone, quartzite and granite concrete. International Journal of Concrete Structures and Materials, Vol. 11, No. 1, March 2017, pp. 17-28.
- [21] Arruda, E. M., S. Ahzi, Y. Li, and A. Ganesan. Rate dependent deformation of semi-crystalline polypropylene near room temperature. Journal of Engineering Materials and Technology, Vol. 119, 1997, id. 216.
- [22] Yogamalar, R., R. Srinivasan, A. Vinu, K. Ariga, and A. C. Bose. X-ray peak broadening analysis in ZnO nanoparticles. Solid State Communication, Vol. 149, 2009, id. 1919.
- [23] Gray, D. E. American institute of physics handbook, Mc Graw-Hill Book Company, New York, 1972.
- [24] Venkateswarlu, K., D. Sreekanth, M. Sandhyarani, V. Muthupandi, A. C. Bose, and N. Rameshbabu. X-ray peak profile analysis of nanostructured hydroxyapatite and fluorapatite. International Journal of Bioscience, Biochemistry and Bioinformatics, Vol. 2, No. 6, 2012, pp. 389-393.
- [25] Rabiei, M., A. Palevicius, A. Dashti, S. Nasiri, A. Monshi, A. D. Akram, et al. X-ray diffraction analysis and Williamson-Hall method in USDM model for estimating more accurate values of stress-strain of unit cell and super cells $(2 \times 2 \times 2)$ of hydroxyapatite, confirmed by ultrasonic pulse-echo test. Materials, Vol. 14, 2021, id. 2949.
- [26] NF EN 196-1. Tests for cements Part 1: determination of strengths, 1995.
- [27] NF EN 1097-6. Essais pour déterminer les caractéristiques mécaniques et physiques des granulats - Partie 6: détermination de la masse volumique réelle et du coefficient d'absorption d'eau, Janvier 2014.